EFFECTS OF A TURBULENT WALL JET OVER A NON-CONFINED BACKWARD-FACING STEP

N. Lancial[1,2,*]
[1] Université Lille Nord-de-France, F-59000 Lille. UVHC TEMPO/DF2T, F-59313 Valenciennes, France
[2] Département TecHnologie Et Modélisation des Infrastructures du Système électrique (THEMIS)
EDF R&D, 92140, Clamart, France
EDF, TEMPO
[*] nicolas.lancial@gmail.com

F. Beaubert[1], **S. Harmand**[1], **T. D. Nguyen**[1], **G. Rolland**[2]

ABSTRACT

Experimental and numerical analysis of a turbulent wall jet downstream of a non-confined backward-facing step are presented. An infrared camera was used to visualize a temperature map of the heated plate downstream the step. A hot wire was utilized to measure the instantaneous local velocity and some PIV/SPIV measures were performed to obtain instantaneous two and three dimensional vector fields. The main objective was to visualize and compare both the fluid flow and the heat transfer, by studying the skin friction coefficient C_f and the Nusselt number Nu_d. The latter is obtained by the calculation of the heat transfer coefficient, evaluated by inverse method. Both experimental data and numerical approach provide good agreement regarding the flow structure and thermal data for measuring the position and the value of characteristics scales in the recirculation zone. Similarities and differences are highlighted in the paper compared to confined configurations.

INTRODUCTION

The physical phenomena of separation and reattachment, involving heat transfer, is commonly encountered in many engineering problems like electrical rotating machines. Calories, which are mostly removed by forced convective transfer, cause local heating in these systems due to poor traffic fluid because of recirculation phenomena. These hot spots can deteriorate the integrity of these structures and act as the origin of electrical faults. Therefore, it is fundamental to understand and analyze this phenomenon. An excellent test for analysing turbulent flows with separation is the study of the backward facing step (Figure 1).

Two flow types appear in confined configuration: free shear flows (flow mixtures with different velocities) and shear flow around obstacles or near walls. The dynamic of the backward-facing step is largely the result of the interaction between them. The turbulent flow features past a confined backward-facing step can be described as follows. A turbulent boundary layer encounters the backward-facing step, the sudden change in surface geometry causes the boundary layer to separate at the sharp step edge. The shear layer, downstream, impinges on the surface and then forms the primary recirculation flow region. The flow impingement is called the reattachment point. This shear layer exists due to a strong, unfavorable pressure gradient. A small counter-rotating corner eddy evolving below the mean recirculation flow might also exist in this area. Downstream of the reattachment, the boundary layer begins to redevelop, followed by the decrease of the scale of the eddies.

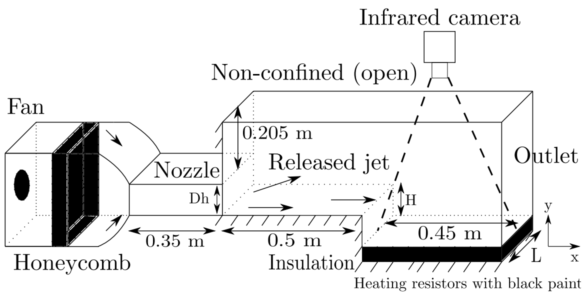

Figure 1. Experimental setup.

Some improvements in the heat transfer predictions with fluid flow, downstream the backward-facing step, have been made in the last decade. According to Boizumault *et al.* (2000), by comparing the fluid dynamics and heat transfer, the shear layer and its impingement downstream the wall are responsible of the variation of the Nusselt number (Nu_d), especially at the reattachment point. Increasing the step height increases the reattachment length, the Nusselt number, the size of the recirculation area and the fluid characteristics in three-dimensions. Vogel & Eaton (1985) and Avancha & Pletcher (2002) have also studied experimentally and numerically turbulent flows involving heat transfer in their studies, and have shown that the peak rate of heat transfer appears upstream of the reattachment point. The latter showing a direct correlation with the maximum of fluctuations in the wall stress.

The backward-facing step has been studied mainly in confined configurations. Few have analyzed a backward-facing step in a non-confined disposition with an upstream wall jet flow and studied the influence of external turbulence structure on the step flow. According to Launder & Rodi (1983) and Nait Bouda *et al.* (2008), the turbulent wall jet presents a particular structure with two centres of

Table 1. Table of the configurations studied.

	D_h (m)	H (m)	L (m)	V_{max} (ms^{-1})	Re_{Dh}=$V_{max}D_h/\nu$
Case *a* - IR / hot wire	0.018	0.015	0.17	19.62	22495
Case *b* - PIV / SPIV	0.021	0.016	0.168	17.2	23006

turbulence production, one because of an inner wall shear layer characterized by small scale eddies, identical to a turbulent boundary layer, and the other one comparable to a free jet outer region of the flow with entrainment of fluid mass characterised by large turbulence scales. Nait Bouda *et al.* (2008) have studied the role of large eddies, especially on the fluctuation of the reattachment point and the decrease of the mean reattachment length. The turbulent plane wall jet can greatly modify the flow structure in the wall region of the step.

The aim of the present work focuses on an experimental and numerical study considering a turbulent wall jet and its interaction downstream of a non-confined backward-facing step. The studied configurations are given in Table 1 and correspond to almost two identical drafts.

The main difference between case *a* and *b* is about the materials used during the experimentation. Bakelite and expanded polystyrene (EPS) which recover lateral surfaces for insulation are used in case *a* to see the effects of the turbulent wall jet on heat transfer. Only plexiglass in lateral surfaces is utilized for PIV measures in case *b*. The Richardson number $Ri_H = Gr/Re_H^2$ shows that the buoyancy does not interact with forced convection as $Ri \ll 1$ (close to 0.00024 for case *a*) and so does not have any influence on the size and the characteristics of the recirculation area as the flow is turbulent according to Safaei *et al.* (2011).

EXPERIMENTAL APPROACH

An infrared camera and a 55P11 hot wire (DANTEC) were used to visualize a temperature map of the heated plate and measure the instantaneous velocity for case *a*, whereas a PIV system (TSI Inc.) was applied to investigate the flow characteristics in case *b*. An electrical transformer was used to apply a constant heating power downstream of the step. The latter was turned off for case *b*.

Before taking temperature measurements from the IR camera, some time was allowed for the establishment of a steady state between the dynamic flows and the thermal conduction (between one to two hours). An average temperature on several images taken from the IR camera has been computed when thermal stability was reached. The global error from the IR camera measures is close to ± 2°C and the maximum error obtained from the hot wire was 1.96% compared to the King law.

IR and hot wire experimental setup - Case a

The infrared camera used during the experiments is a Jade III MWIR (InSb). The main characteristics of the IR camera are its spectral range, between 3.6 μm and 5.1 μm, its pixel pitch, close to 30 μm. Its image format is given by 320*240 pixels for a digital frequency near 194 Hz. A lens with a 50 mm focal length is used. The same field of view and spatial resolution were kept for all the experiments. Its pixel clock is equal to 16 MHz. The sensitivity is about 4.28 mK/DL for a temperature close to 25-26°C. The range of temperature used during the experiments are from 20°C to 40°C and from 35°C to 100°C. The IR camera is located above the backward-facing step at 1.8 m.

A specific 55P11 hot wire was used to measure the velocity. It is a single-sensor wire-probe along the flow direction. The measurements were performed with 2048 samples at 0.6 kHz. The sampling interval for each average velocity was 3.413 s. It provides instantaneous velocity, which is useful for measuring turbulent fluctuations. It produces negligible disturbances upward from the measurement point. We can note that a special care was given for measuring the velocity to obtain a good calculation of the turbulence intensity. The range of the latter is between 5.51% (near walls) and 2.33% (in the middle plane section) at the nozzle exit.

Identification procedure of the heat transfer

In this problem, temperature measurements can be utilized to identify surface conditions, such as convective heat fluxes, using the inverse method. We have focused our attention on solving a steady 1D problem because the thermal stability is reached and the flow can be considered homogeneous in the transverse direction. This model can determine the value of the local wall heat flux, φ. The equation is:

$$p + \lambda \frac{\partial^2 T}{\partial x^2} = \frac{1}{e}\varphi \tag{1}$$

The inverse method allows the distribution of φ to be determined by comparing the computed with the average measured temperature. As explained by Tikhonov & Nikolayevich (1963), this model involves searching for the distribution of φ that will minimize the following function for each iteration n. The difference between the measured temperature T_{mes} and the temperature T_{cal}, calculated by inverse method, should tend to zero. However, the minimization of this equation can cause the amplification of errors in input data. Some regularization terms are so added, but one has strong influence on the final results, denoted as α_1. It minimizes the effect of noise measurements on the identified local wall heat flux φ. It limits its important variations and so generate the most stable solution to accurately solve it. A new function can be defined, denoted as S:

$$S = \sum_x \left[T_{cal}^n(x) - T_{mes}(x)\right]^2 + \alpha_1 \sum_x \left[\overrightarrow{grad}\left(\varphi^n(x)\right)\right]^2 \tag{2}$$

During the iterative process, the local wall flux at the iteration $n+1$, φ^{n+1}, is determined knowing φ^n at the iteration n. The function F is minimized as:

$$\varphi^{n+1} = \varphi^n + \triangle\varphi \tag{3}$$

with:

$$\triangle\varphi = -\left\{[J]\,[J]^t + \alpha_1\,[X]\right\}^{-1} \times \left\{[J]\left(\left[T^n_{cal}\right][\varphi^n] - [T_{mes}] + \alpha_1\,[X]\,[\varphi^n]\right)\right\} \quad (4)$$

and

$$[J] = \left[\frac{\partial T^n_{cal}}{\partial \varphi^{n+1}}\right]$$

$$[X] = \frac{1}{2}\left[\frac{\partial S_1}{\partial \varphi^{n+1}}\right]\left[\varphi^{n+1}\right]^{-1}$$

$$S_1 = \Sigma_i \left[\varphi^{n+1}_{i+1} - \varphi^{n+1}_i\right]^2$$

In general, for $\alpha_1 = 0$, the plot of the heat transfer coefficient will be very noisy and will fluctuate, whereas, for α_1^{opt}, the diagram will be smoothed as accurately as possible. The optimal values of α_1 correspond to the optimum of the matrix $\left([J]\,[J]^t + \alpha_1\,[X]\right)$, namely:

$$cond\left([J]\,[J]^t + \alpha_1^{opt}\,[X]\right) = min\left\{cond\left([J]\,[J]^t + \alpha_1\,[X]\right)\right\} \quad (5)$$

The iterative process is stopped when value of the function S remains constant in two successive iterations.

PIV experimental setup - Case b

The PIV system consisted of a New Wave Nd:YAG laser (TSI Inc.) with an articulated light arm, digital charge couple device (CCD) cameras, a synchroniser and a computer. The Nikkor camera lens had a 105-mm focal length and an f/5.6 aperture. Each laser bean of the double-pulsed laser was capable of 200 mJ/pulse at a wavelength of 532 nm. These beams were adjusted by a cylindrical and a spherical lens to form a 1-mm-thick laser sheet. The laser sheet thickness, as proposed by Raffel *et al.* (2007), is optimised to be thin enough to generate adequate particle intensity but thick enough to reduce the loss of particle image pairs. An olive oil droplet generator (TSI 9307) generated particles with a mean diameter of 1 μm to seed the inlet of the backward-facing step jet. The TSI PowerView Plus 4MP cameras with a resolution of 2.048×2.048 pixels and a pixel size of 7.4×7.4 μm^2 captured PIV/SPIV images and directly sent them to the computer. A LaserPulse (TSI Model 610035) synchroniser controlled the synchronisation between the lasers and cameras. Depending on the jet velocity, the time interval between the first and the second exposures varied from 15 to 30 μs.

In this configuration, we performed PIV and stereoscopic-PIV (SPIV) measurements along the axial and the transversal direction namely from the outlet of the nozzle and from the backward-facing step. PIV images were separately captured in these different regions with similar flow conditions. Sequences of 1000 and 2000 images were respectively recorded for the PIV and SPIV measurements with a sampling rate of 1 Hz. The velocity fields obtained from the PIV and SPIV image pairs were checked to be statistically independent. Image acquisition and image processing were performed with TSI Insight TM 4G software. The interrogation window of 32×32 pixels is applied. We analysed the PIV and SPIV images by using a recursive Nyquist rectangular grid algorithm with two iterations and a 50% window overlap. The first iterations started with an interrogation window of 64*64 pixels while the second iterations ended with an interrogation window of 32*32 pixels. For all the tests, the percentage of bad vectors, which was calculated as the average over the number of PIV/SPIV velocity fields, was about 3%.

NUMERICAL APPROACH

Experimental data from case *a* are compared to flow modeling which was performed using CFD software Code_Saturne. We have compared RANS (k-ω SST and $v_2 f$) and LES model using the Dynamic Smagorinsky subgrid scale model, as proposed by Germano *et al.* (1991), with experimental data. A thermal model was implemented in Code_Saturne to see the interaction between the fluid flow and heat transfer (EDF (2011)). The coupling with heat transfer was performed with SYRTHES, version 4.0 (Rupp & Peniguel (2007)).

At the inlet of the computational domain ($x/D_h = -27.78$), a mean velocity profile was applied by following the 1/7 power law. Upstream, the nozzle length (0.35 m) was sufficient to ensure fully developed flow. It was verified that the velocity and turbulence intensity values at the nozzle outlet were similar to experimental data. A non-slip boundary and a symmetry conditions were used, respectively, on the wall and at the top of the domain. A constant pressure profile was imposed at the outlet. The upstream flow is considered here to be bidimensional, which means that the hydraulic diameter can be assumed to be twice the height of the nozzle. The reference temperature was taken equal to the room temperature, namely at 23.5°C. The walls are considered adiabatic. The true power injected into the plate was 167.2 W, by taking into account the losses.

A geometry sensitivity test was performed in 2D and 3D. An artificial growth of the geometry at the top and the exit was performed in order to prevent disturbances from the boundary conditions in the zone of interest. A mesh sensitivity test was performed as well for both. For all of our simulations, the cell sizes in wall units were in the range of $\triangle x^+ < 30$, $\triangle y^+ \simeq 1$, $\triangle z^+ < 30$. It enables to capture the viscous sub-layers and obtain a good estimate of the wall heat transfer for the k-ω SST model.

RESULTS AND ANALYSIS

In this study, the expansion ratio was $ER = 1.2$ and $ER = 1.3$ and the aspect ratio of the backward-facing step was equal to $AR = 11.33$ and $AR = 10.5$ for case *a* and case *b*, respectively. The tri-dimensional effect could be neglected as proposed by De Brederode & Bradshaw (1972).

Results obtained from case a

Figure 2 compares the numerical and experimental mean streamwise velocity profiles downstream of the step. Globally, we can assume that a satisfactory agreement between the experimental results and the numerical predictions is achieved, especially with the LES code near walls: it precisely determines the flow structure there. For the RANS model, the k-ω SST turbulence model gives better results than the $v_2 f$ φ-model, which overestimates $< V_x > /V_{max}$ values more than 25%.

Figure 3 shows the flow pattern downstream of the step. A main recirculating loop is clearly observed and a

Table 2. Comparison of the different hot spot values.

	Exp.	Coupling v_2f φ-model	Coupling k-ω SST	$< LES >$
Position - x/D_h	0.511	0.25	0.5	0.611
Relative error - %	-	51.1	2.2	19.5
T_{max} - °C	63.5	55.4	66.9	76.7
Temperature difference - °C	-	-8.1	3.4	13.2

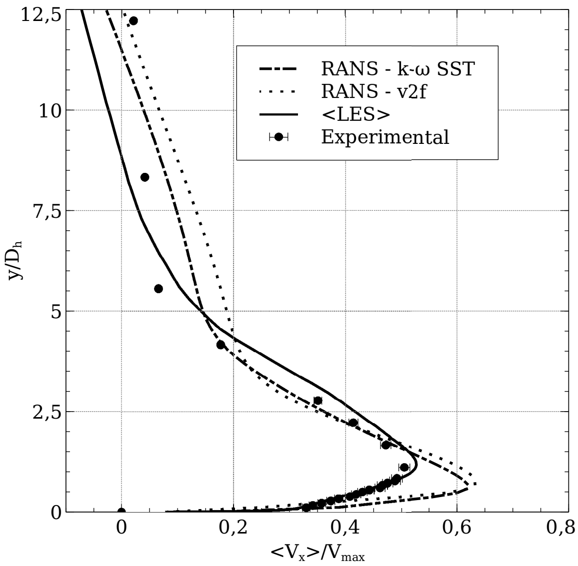

Figure 2. Vertical velocity distribution for x/D_h=4.98 downstream of the step.

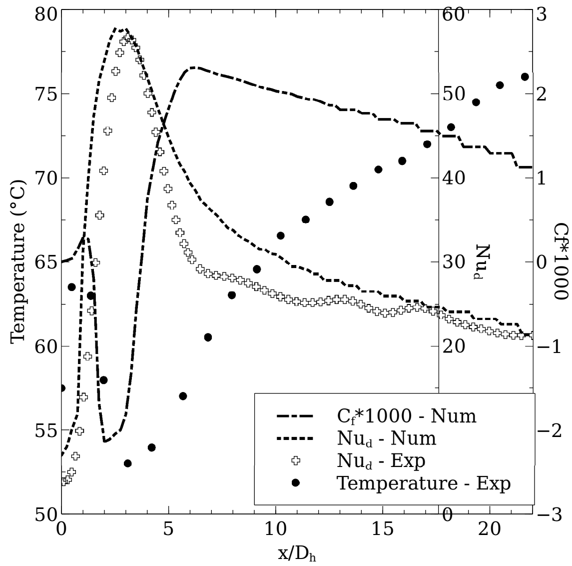

Figure 4. Comparison between the skin friction coefficient C_f obtained by numerical simulation (coupling k-ω SST) with the temperature and Nusselt number (centerline).

secondary recirculation bubble also exists near the step corner. The small bubble is counter clockwise and extends approximately 0.8D_h (0.96H) in length in the streamwise direction and 0.5D_h (0.6H) in the wall normal direction. The large main recirculating loop is clockwise and has a length close to 1.8D_h (2.16H) in the x-direction and 0.7D_h (0.84H) in the y-direction. It is limited above by the separating flow. A similar flow pattern was observed by Nait Bouda *et al.* (2008) in a configuration corresponding to an incoming wall jet flow with $ER = 2$.

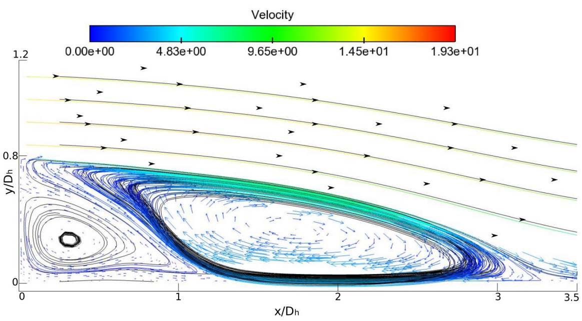

Figure 3. Numerical prediction of the flow pattern downstream of the step (streamlines of the mean flow).

The coupling of Code_Saturne and SYRTHES with the k-ω SST turbulence model gives better temperature results compared to experimental values than other models, about the position and the value of the maximum temperature, T_{max} (see Table 2). For the LES model, there is a 19.5% relative error compared to the experimental data on the hot spot position. The latter can so be described by both the experimental and numerical studies.

The location of the hot spot is well given by the thermal analysis as we can see more precisely in Figure 4. Close to the step, the velocity is small involving a maximum temperature and a minimum Nusselt number. More conclusions can be given for the location of the reattachment point, defined by $C_f = 0$ (see Figure 4), where the temperature is minimum and the Nusselt number is maximum. We can note that, experimentally, it was difficult to precisely obtain $C_f = 0$ with the hot wire. The Nusselt number, given by experimental or by numerical data, gives the same tendency about the value of Nu_{max} and Nu_{fd}. We can note that, experimentally, the correlation between the temperature and the Nusselt number is not so obvious due to the use of the inverse method, which does not guarantee the same trend.

Table 3 presents a comparison between the locations of C_f (obtained by numerical simulation) and the lowest temperature T_{min}. Numerically the reattachment length is obtained from the location of the zero skin friction coefficient C_f. It is close to 3.61D_h (4.33H) for the k-ω SST model

Table 3. Comparison between fluid flow (C_f obtained by numerical approach) and heat transfer (T°) at the reattachment point.

	Exp.	Coupling v_2f φ-model	Coupling k-ω SST	$< LES >$
Position of $C_f = 0$ - x/D_h	-	4.056	3.611	3.5
Position of T_{min} - x/D_h	3.089	5.25	3	3.056
Relative error - %	-	69.9	2.9	1.1
T_{min} - °C	53	50.25	63.2	47.2
Temperature difference - °C	-	-2.75	10.2	-5.8

and $3.5D_h$ (4.2H) for the LES simulation. The numerical prediction of the reattachment length depends on the upstream flow conditions. Therefore, with $ER = 1.2$, our reattachment length is below 5H and does not correspond to the values found for the confined backward-facing step (Adams & Johnson (1988)). For comparison with a similar configuration, Nait Bouda *et al.* (2008) found a mean of 4.5H. They attributed it to the additional turbulent diffusive transfer due to the energetic motions of the eddies in the external flow layer. Globally, we can assume that a satisfactory agreement between the experimental results and the numerical predictions is achieved, especially with the LES code near walls: it precisely determines the flow structure there.

A comparison can be done between the position of the maximum heat transfer position x_{max} and the reattachment position x_r, obtained from the numerical simulation. The following equations are found: $x_{max} = 0.83 \times x_r$ and $x_{max} = 0.87 \times x_r$, by using the coupling k-ω SST and LES models, respectively. In a confined configuration, the position x_{max} of the maximum Nusselt number Nu_{max} is correlated to the mean reattachment point x_r by the relation: $x_{max} = 0.9 \times x_r$, as proposed by Vogel & Eaton (1985) and Boizumault *et al.* (2000), for a turbulent flow. Consequently, the value of the constant is slightly smaller for a non-confined study, according to numerical values. Moreover, a correlation can also be done between the minimum of $C_{f_{min}}$ and the reattachment position x_r, namely: $C_{f_{min}} = 0.55 \times x_r$ and $C_{f_{min}} = 0.57 \times x_r$, by studying the same numerical models. It is different compared to the confined studies, where Jovic & Driver (1995) show that the minimum skin friction coefficient $C_{f_{min}}$ occurs at a distance of approximately 2/3 x_r. It is also different from the non-confined study of Nait Bouda *et al.* (2008) with upstream wall jet configuration, where it was found that its location is much closer to the reattachment point. More precision is given in next section. Finally, the LES model is closer to the experimental data than the RANS with or without a thermal coupling for obtaining the position of the lowest temperature T_{min}. Furthermore, the coupling v_2f φ-model gives the best results for the minimum in the temperature because this model was originally developed for an impinging jet, attached or mildly separated boundary layers. However, in the recirculation area, it does not give satisfactory results. Both the flow structure and thermal data provide good agreement to measure the positions and the values of characteristics areas downstream the step.

Results obtained from case b

Figure 5 presents the mean velocity and the turbulent kinetic energy fields in streamwise direction at the inlet.

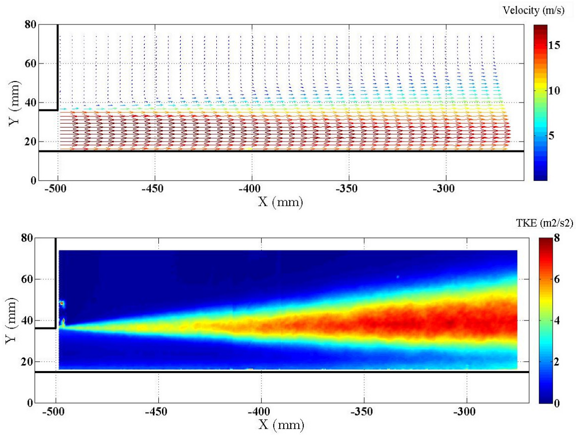

Figure 5. Representation of the mean velocity and the TKE in streamwise direction at the nozzle exit.

We can see that considering a turbulent wall jet instead of a standard boundary layer behaves like a classical turbulent boundary layer in the inner while the external turbulent large eddies produce real changes in the dynamics of the flow, like a free jet as proposed by Nait Bouda *et al.* (2008).

Figure 6 shows the contours of the streamwise velocity and the root mean square fluctuating streamwise velocity in the transversal direction at the nozzle exit obtained by SPIV measure.

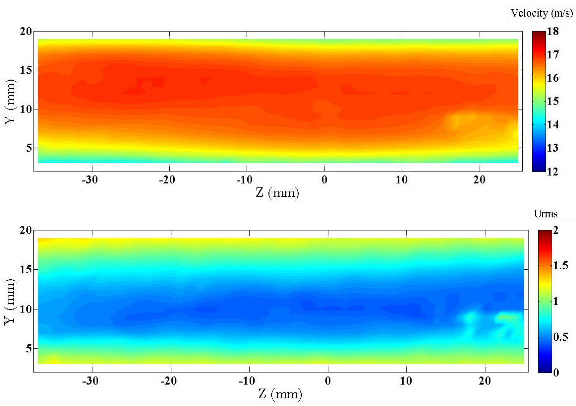

Figure 6. Representation of the mean streamwise velocity and the root mean square fluctuating streamwise velocity at the nozzle exit in transversal direction.

The mean streamwise velocity and the root mean square fluctuating velocity are presented. The flow seems to be globally symmetrical due to the confinement: it confirms that the tri-dimensional effects could be neglected as proposed by De Brederode & Bradshaw (1972).

The mean velocity and the turbulent kinetic energy can be plotted downstream the step, respectively in Figure 7.

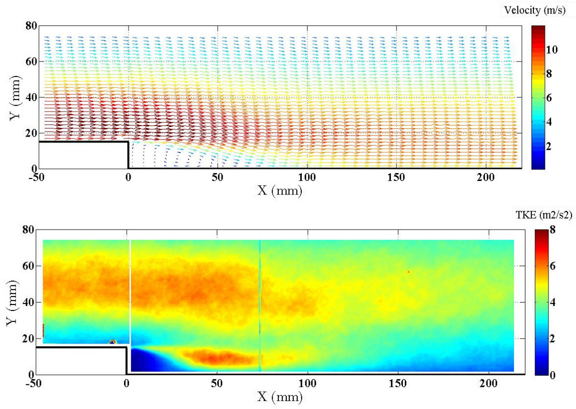

Figure 7. Representation of the mean velocity and the turbulent kinetic energy downstream the backward-facing step.

The flow structure in the wall region of the step is considerably modified by the presence of the turbulent wall jet at the nozzle exit, as shown in Figure 3. As it was noticed in the previous case with similar configuration, the reattachment length is also below 5H. The large eddies in the free boundary, which interacts with the separated recirculating zone, modify the flapping of the impingement of the jet on the wall, making the mean reattachment length to decrease and can explain the relations between x_{max}, $C_{f_{min}}$ and x_r.

CONCLUSION

This study analyses the influence of a turbulent wall jet flow downstream of a non-confined backward-facing step.

The conjugate heat transfer computations, which were performed by coupling the thermal (SYRTHES) and flow (Code_Saturne) codes give the best results for the position and capture of the hot spot compared to the experimental study in case *a*, especially with the k-ω SST turbulence model. The LES model gives the best results to capture the fluid flow and to follow the position and the value of the lowest temperature. Both the experimental data and numerical simulation (except for the coupling v_2f φ-model) catch well the position of these points. Some comparisons between the skin friction coefficient C_f (obtained by numerical simulation), the temperature and the Nusselt number Nu_d at the hot spot and at the reattachment point were given. Both the flow structure and thermal data provide good agreement to measure their positions and their values.

Some results found in this paper have been compared to confined configurations. The range of the reattachment point location is between 4.2H and 4.33H which is shorter than those generally found in a confined backward-facing step. The correlation between the position of the maximum heat transfer position x_{max} and the reattachment position x_r is slightly different according to numerical approaches. The same conclusion can be made for the correlation between the minimum of $C_{f_{min}}$ and the reattachment position x_r.

The results obtained by PIV/SPIV measurements enable to better understand the impact of a turbulent wall jet downstream the backward-facing step. The external turbulent large eddies produce real changes in the dynamics of the flow, upstream and downstream the step.

ACKNOWLEDGEMENTS

The authors are grateful for the financial support provided by the MEDEE project, the Région Nord Pas-de-Calais, European project FEDER and the French National Research Agency.

REFERENCES

Adams, E.W. & Johnson, J.P. 1988 Effects of the separating shear layer on the reattachment flow structure. *Pressure & turbulent quantities, Expts. In Fluids* **6**, 400–408.

Avancha, R.V.R. & Pletcher, R.H. 2002 Large eddy simulation of the turbulent flow past a backward-facing step with heat transfer and property variations. *International Journal of Heat and Fluid Flow* pp. 601–614.

Boizumault, F., Harmand, S. & Desmet, B. 2000 Influence of the characteristics of an aerodynamically perturbed flow on the local heat transfer by convection from a wall. *International Journal of Heat and Mass Transfer* **43**, 791–806.

De Brederode, V. & Bradshaw, P. 1972 Three-dimensional flow in nominally two-dimensional separation bubbles. i. flow behind a rear-ward-facing step. Aeronautical report. Imperial College.

EDF 2011 Code saturne 2.1 theory and programmer's guide. Manual. EDF R&D, 6 quai Watier, F78401 CHATOU Cedex.

Germano, M., Piomelli, U., Moin, P. & Cabot, W.H. 1991 A dynamic sub-grid scale eddy viscosity model. *Physics of Fluids* pp. 1760–1765.

Jovic, S. & Driver, D. 1995 Reynolds number effect on the skin friction in separated flows behind a backward-facing step. *Experiments in Fluids* pp. 464–467.

Launder, B.E. & Rodi, W. 1983 The turbulent wall jets - measurements and modeling. *Annual Review of Fluid Mechanics* **15**, 429–459.

Nait Bouda, N., Schiestel, R., Amielh, M., Rey, C. & Benabid, T. 2008 Experimental approach and numerical prediction of a turbulent wall jet over a backward-facing step. *International Journal of Heat and Fluid Flow* pp. 927–944.

Raffel, M., Willert, C., Wereley, S. & Kompenhans, S. 2007 Particle image velocimetry: a practical guide. Manual - springer. Imperial College, Berlin.

Rupp, I. & Peniguel, C. 2007 Syrthes 4.0 - user guide. Manual. EDF R&D, Chatou, France.

Safaei, M.R., Goshayeshi, H.R., Razavi, B.S. & Goodarzi, M. 2011 Numerical investigation of laminar and turbulent mixed convection in a shallow water-filled enclosure by various turbulence models. *Scientific Research and Essays* **6**, 4826–4838.

Tikhonov & Nikolayevich, A. 1963 On the stability of inverse problems. *Doklady Akademii Nauk SSSR* pp. 195–198.

Vogel, J.C & Eaton, J.K. 1985 Combined heat transfer and fluid dynamic measurements downstream of a backward facing-step. *Journal of Heat Transfer* **107**, 922–929.